Spring Snow-Albedo Feedback Analysis Over the Third Pole: Results From Satellite Observation and CMIP5 Model Simulations

Hui Guo, Xiaoyi Wang, Tao Wang, Yaoming Ma, James Ryder, Taotao Zhang, Dan Li, Jinzhi Ding, Yue Li, Shilong Piao

AGU PUBLICATIONS

JGR

Journal of Geophysical Research: Atmospheres

RESEARCH ARTICLE
10.1002/2017JD027846

Hui Guo and Xiaoyi Wang contributed equally to this work.

Key Points:
- Snow metamorphosis feedback determines present-day spring snow-albedo feedback in Karakoram, but not found in Southeastern Tibet
- Altitudinal distribution of present-day snow-albedo feedback strength is in accord with that of the warming rate for the last three decades
- The future snow-albedo feedback over Karakoram is nearly 1.5 and 3 times as strong as that over Southeastern Tibet and the Third Pole

Supporting Information:
- Supporting Information S1

Correspondence to:
T. Wang,
twang@itpcas.ac.cn

Citation:
Guo, H., Wang, X., Wang, T., Ma, Y., Ryder, J., Zhang, T., … Piao, S. (2018). Spring snow-albedo feedback analysis over the third pole: Results from satellite observation and CMIP5 model simulations. *Journal of Geophysical Research: Atmospheres*, *123*, 750–763. https://doi.org/10.1002/2017JD027846

Received 6 OCT 2017
Accepted 29 DEC 2017
Accepted article online 5 JAN 2018
Published online 18 JAN 2018

Spring Snow-Albedo Feedback Analysis Over the Third Pole: Results From Satellite Observation and CMIP5 Model Simulations

Hui Guo[1,2], Xiaoyi Wang[1], Tao Wang[1,3], Yaoming Ma[3,4], James Ryder[5], Taotao Zhang[1,2], Dan Liu[1], Jinzhi Ding[1], Yue Li[6], and Shilong Piao[1,3,6]

[1]Key Laboratory of Alpine Ecology and Biodiversity, Institute of Tibetan Plateau Research, Chinese Academy of Sciences, Beijing, China, [2]University of Chinese Academy of Sciences, Beijing, China, [3]CAS Center for Excellence in Tibetan Plateau Earth Sciences, Chinese Academy of Sciences, Beijing, China, [4]Key Laboratory of Tibetan Environment Changes and Land Surface Processes, Institute of Tibetan Plateau Research, Chinese Academy of Sciences, Beijing, China, [5]Laboratoire des Sciences du Climat et de l'Environnement (LSCE/IPSL), CEA-CNRS-UVSQ, Université Paris-Saclay, Gif-sur-Yvette, France, [6]Sino-French Institute for Earth System Science, College of Urban and Environmental Sciences, Peking University, Beijing, China

Abstract The snow-albedo feedback is a crucial component in high-altitude cryospheric change but is poorly quantified over the Third Pole, encompassing the Karakoram and Tibetan Plateau. Here we present an analysis of present-day and future spring snow-albedo feedback over the Third Pole, using a 28 year satellite-based albedo and the latest climate model simulations. We show that present-day spring snow-albedo feedback strength is primarily determined by the decrease in albedo due to snow metamorphosis, rather than that due to reduced snow cover in the Karakoram, but not found in Southeastern Tibet. We further demonstrate an emergent relationship between snow-albedo feedback from the seasonal cycle and that from climate change across models. Combined with contemporary satellite-based snow-albedo feedback from seasonal cycle, this relationship enables us to estimate that the feedback strength for the Karakoram with a relatively high glaciated area is $-2.42 \pm 0.48\%\ K^{-1}$ under an unmitigated scenario, which is much stronger than that for Southeastern Tibet ($-1.64 \pm 0.48\%\ K^{-1}$) and for the Third Pole ($-0.89 \pm 0.44\%\ K^{-1}$), respectively. Moreover, it is noteworthy that the magnitude of the constrained strength is only half of the unconstrained model estimate for the Third Pole, suggesting that current climate models generally overestimate the feedback of spring snow change to temperature change based on the unmitigated scenario.

1. Introduction

Snow-albedo feedback, quantified as the change in surface albedo per unit change in near-surface air temperatures (Qu & Hall, 2007, 2014), is a measure of the further increase in temperature due to the initial warming-induced increase in absorbed solar radiation when snow retreats (Wallace, 1992). This feedback is widely acknowledged as the main cause for accelerated climate change in the Northern Hemisphere (Groisman et al., 1994) and is ranked as the second largest contributor to amplified warming in the Arctic over the last 30 years (Pithan & Mauritsen, 2014). In contrast, the snow-albedo feedback over the Third Pole, which harbors the largest area of snow and glaciers in the midlatitudes, is poorly quantified (Xu et al., 2009; Yao et al., 2012). This lack of precision constitutes a major source of uncertainty in the assessment of recent dramatic cryospheric changes.

The importance of snow cover on climate has been widely recognized over the Third Pole; for example, snow changes can profoundly affect the strength of the East and the South Asian Monsoon (Blanford, 1884; Fasullo, 2004; Seol & Hong, 2009) and the winter climate in Canada (Lin & Wu, 2012) through thermal forcing. Furthermore, characterizing snow-albedo feedback and its drivers should also improve our understanding of current hot topics in recent climate change research on the Third Pole.

First of all, in consistent with historical observations in the Arctic, climate change has been amplified in the Third Pole over the last few decades (Kang et al., 2010; Ma et al., 2011; Rangwala & Miller, 2012; Zhong et al., 2011). Moreover, due to its location in the midlatitudes, the Third Pole has a higher loading of surface solar radiation than does the Arctic. A comparable unit change in surface albedo (and in absorbed solar

radiation) might well have a stronger temperature feedback in the Third Pole than it would do in the Arctic. The snow-albedo feedback quantification therefore sheds light on the difference in the recent temperature amplification that occurs in both regions. Second, there is growing evidence that the rate of recent warming is amplified with elevation. The snow-albedo feedback is proposed as the most important mechanism underlying the observed elevation-dependent warming (X. D. Liu et al., 2009; Pepin et al., 2015; Qin et al., 2009; Zeng et al., 2015). The Third Pole, including the most extensive high elevation area such as the Karakoram, Himalayas, and Tibetan Plateau (Qiu, 2008), is therefore an ideal region in which to explore the linkage between elevation-dependent warming (i.e., greater warming at higher elevations than at lower elevations) and altitudinal distribution of snow-albedo feedback strength (Yan et al., 2016). Third, the status of glaciers displays systematic different behaviors over the last three decades, with glaciers shrinking in most of the Himalayas and advancing in the Karakorum (this is known as the "Karakorum anomaly") (Picard et al., 2012; Yao et al., 2012). It is suggested that these differences are driven by different trends in precipitation deposition (mainly as snowfall) on the glacier surface (Yao et al., 2012), which might determine the magnitude of the snow-albedo feedback (Picard et al., 2012) and in turn the glacier status. These growing hot topics in climate change research highlight the necessity of a data-based study to quantify the snow-albedo feedback over the Third Pole.

A quantitative understanding of future snow-albedo feedback is pivotal to developing confidence in the constrainment of climate change projections on the Third Pole. Earth system models are a direct way to estimate future snow-albedo feedback, but there is a large model spread in simulations of snow-albedo feedback in the Coupled Model Intercomparison Project versions 3 (CMIP3) and 5 (CMIP5) (Cox et al., 2013; Fletcher et al., 2015; Li et al., 2016). However, there is a powerful emerging constraint approach which can help determine future snow-albedo feedback, based on model projections and observations (Cox et al., 2013; Kwiatkowski et al., 2017; Wenzel et al., 2016; Zhao et al., 2017). This technique utilizes the potential emerging intermodel relationship between snow-albedo feedback from the seasonal cycle and that from future climate change (Hall & Qu, 2006), which is then constrained by the snow-albedo feedback observed over the current seasonal cycle, in order to estimate snow-albedo feedback in future climate change. The application of this approach in constraining future modeled snow-albedo feedback could provide insights over the Third Pole into issues that are now highly topical. For example, will the current regional differentiation in cryospheric change persist into the future, or will there be an acceleration in the rate of future temperature change? The objectives of this paper are therefore to quantify snow-albedo feedback strength during the course of the last 30 years and estimate observational-constrained future snow-albedo feedback over the Third Pole, using long-term satellite-derived snow cover, albedo products, and ancillary climate data, in conjunction with an ensemble of CMIP5 models.

2. Data Sets and Methods

2.1. Observation-Based Data Sets

The long-term (1982–2009) time series of black-sky surface albedo data used here are from CLARA-A1-SAL (CLoud, Albedo and RAdiation data set first release-Surface ALbedo) that is constructed based on the homogenized Advanced Very High Resolution Radiometer (AVHRR) radiance data. These albedo data are generated by the Satellite Application Facility on Climate Monitoring (CMSAF) (referred hereafter as CMSAF albedo) and are available at a spatial resolution of 0.25° and a temporal resolution of 5 days, on a global scale. The product goes through a series of topographical, atmospheric, and anisotropic corrections in order to remove various deleterious effects, such as shifted geolocation and aerosol contamination (see details in http://www.cmsaf.eu). The retrieved albedo data are defined over a wave band of 0.25–2.5 μm (0.35–2.8 μm for snow), and the retrieval accuracy for snow and ice in general is found to be 5–15% (in relative units) (Karlsson et al., 2013). It is essential to mention here that this albedo product has been successfully adopted to study albedo trend and its potential drivers in the Arctic sea ice zone during the period 1982–2009 (Karlsson et al., 2013).

To evaluate the applicability of CMSAF albedo over the Third Pole, we use in situ albedo that is calculated as the ratio of in situ shortwave radiation values measured upward to downward at three sites on the Tibetan Plateau: NAMOR (Nam Co Station for Multisphere Observation and Research), QOMS (Qomolangma Station for Atmospheric and Environmental Observation and Research), and SETS (Southeast Tibet Station for

Alpine Environment Observation and Research) (Table S1 in the supporting information). At these sites, the radiometers used to sample the radiation data are deployed over a flat terrain, and the land cover is homogeneous at a 1 km spatial scale (Qin et al., 2011). To be comparable with CMSAF albedo, in situ recorded hourly albedo data are averaged to corresponding values at intervals of 5 days. To acquire the albedo from the CMSAF for each site, we use the albedo of the grid cell (~25 km) in which stations located. We should inform that the CMSAF albedo is the black-sky surface albedo (i.e., the incoming radiation flux is the direct radiation flux without any atmospheric effects), while in situ measured albedo is all-sky surface albedo (i.e., the incoming radiation flux is a weighted combination of direct and diffuse radiation fluxes depending on the cloudiness, atmospheric characteristics, and Sun zenith angle). We might not expect that this issue could significantly bias the albedo comparison between CMSAF and in situ albedo, since the difference between black-sky and all-sky albedo is documented to be rather small (J. C. Liu et al., 2009; Manninen et al., 2012). Furthermore, to evaluate the robustness of CMSAF albedo, we also use the MODIS BRDF/Albedo (MCD43B3, version5) product with a spatial resolution of 500 m, which is widely used as the benchmark for other satellite-derived albedo products (He et al., 2014). Note that only the albedo data flagged as the high quality are considered in this study.

The snow cover extent data during the period 1982–2009 are taken from the weekly National Oceanic and Atmospheric Administration/National Climatic Data Center (NOAA/NCDC) Climate Data Record of Northern Hemisphere snow cover extent data (1979–2010) (Robinson et al., 2012), at a spatial resolution of 25 km. The snow cover extent data set is generated based on the visual interpretation of AVHRR, GOES, and other visible-band satellite data (Helfrich et al., 2007) and is found to have a 95% confidence interval uncertainty in a snow cover fraction of 3–5% during the Northern Hemisphere spring over the period 1966–2010 (Brown & Robinson, 2011). This weekly SCE product is a gridded data set and also provides a binary value for each grid cell, with 1 and 0 indicating snow covered and snow free, respectively. We therefore assume that the binary values 1 and 0 from NOAA SCE product correspond to 100% and 0% snow cover fraction at the weekly time interval, respectively. For a given month, the monthly snow cover fraction is then obtained from averaging weekly snow cover fraction within this month. It is a challenge to map snow cover from satellite measurements over the Third Pole due to its complex topography and frequent cloud cover. Since the NOAA snow data set is produced mainly from visual interpretation of visible satellite imageries by analysts, we here use the MODIS/Terra snow cover L3 Global data set (MOD10CM, version 6) to evaluate NOAA snow cover data over the Third Pole. The use of MODIS snow cover fraction as the validation data set is further evidenced by the study of Pu et al. (2007), which, through comparing the data with in situ snow observations, determined that the overall accuracy of MODIS snow cover fraction can reach as high as ~90% over the Tibetan Plateau.

Monthly temperature data at a spatial resolution of 0.5° × 0.5° covering the period 1982–2009 are compiled from the data sets of the Climate Research Unit, University of East Anglia (CRU TS3.2) (Mitchell & Jones, 2005; New et al., 1999). Note that all available data sets above are resampled to a 0.25° grid using the first-order conservative method (https://code.zmaw.de/projects/cdo). The elevation data are taken from the Shuttle Radar Topography Mission digital elevation data (SRTM 90 m) that were originally produced by NASA (http://srtm.csi.cgiar.org/SELECTION/inputCoord.asp).

2.2. ERA-I Reanalysis and Climate Model Simulations

Because of the harsh environment and data scarcity over the Third Pole, the reanalysis products are widely used to understand the interactions between atmosphere and cryosphere (e.g., Kumar et al., 2015; Ménégoz et al., 2014; Yang et al., 2016), especially ERA-Interim (Dee et al., 2011). It is therefore important to have a quantitative understanding of ERA-I performance in simulating snow-albedo feedback. But we should be aware that compared to other regions such as Europe and Russia, there are only a few snow stations from the Third Pole that are included in ERA-I snow assimilation system. We therefore use monthly surface albedo, snow depth, snow density, snowfall, and air temperature at 2 m from the latest ERA-I reanalysis. It is produced by a sequential data assimilation scheme developed in the European Centre for Medium-Range Weather Forecasts (ECMWF) (Dee et al., 2011). It has a spatial resolution of 0.25° and spans the period 1982–2009. Specifically, snow variables (snow depth and snow density) are first estimated by the ECMWF forecast model, and then updated based on a Cressman analysis of snow depth observations from a synoptic observations station network and satellite-based snow cover data from the daily Interactive Multisensor (Drusch

et al., 2004). Since Snow Cover Fraction (SCF) is not available in ERA-I, we adopt the satellite-derived SCF formulation from Niu and Yang (2007) to calculate SCF from snow depth and snow density.

$$\mathrm{SCF} = \tanh\left(h_{\mathrm{sno}}/\left[2.5Z0_g \times (\rho_{\mathrm{sno}}/\rho_{\mathrm{new}})^m\right]\right) \quad (1)$$

where *h*sno is snow depth, Z0g (=0.01 m) is the ground roughness length, ρsno represents snow density, ρnew is the fresh snow density (100 kg m^{-3}), and *m* is a melting factor (*m* = 1). The monthly ERA-I data can be downloaded from the ECMWF data server (http://ecmwf.int/en/research/climate-reanalysis/erainterim).

We also use Earth system models (ESMs) participating in the fifth phase of the Coupled Model Intercomparison Project (CMIP5) (Taylor et al., 2012), since the assessment of the performance of CMIP5 models enables us to understand the uncertainty and robustness of models in projecting future climate change due to changes in snow cover over the Third Pole. The decision as to which ESMs are considered depends on whether all principle variables are available. These variables include monthly air temperature at 2 m, surface downwelling shortwave radiation, surface upwelling shortwave radiation, snow quantity, and snow depth. Based on this criterion, 26 ESMs in total are selected from the CMIP5 repository (Table S2). In addition, the main characteristics of snow modeling in CMIP5 models are also displayed in terms of the snow layering scheme and in terms of the parameterizations related to snow density and snow-covered albedo (Table S2). The historical simulation during the period 1982–2005 and future climate change simulation under the unmitigated scenario during the period 2070–2095 are used in this study. The unmitigated scenario referring to RCP8.5 scenario corresponds to total anthropogenic radiative forcing estimated to be 8.5 W m^{-2} in the year 2100. Surface albedo is calculated as the ratio of surface upwelling shortwave radiation to surface downwelling shortwave radiation. SCF is inferred based on equation (1). Given that the majority of the models have multiple ensemble members, we take the ensemble mean over all available realizations for each model. All ESMs outputs are resampled to 0.25° × 0.25° using the first-order conservative remapping scheme, as implemented by Climate Data Operators (https://code.zmaw.de/projects/cdo).

2.3. Calculation of Snow-Albedo Feedback and the Two Components

Following the same methodology as Qu and Hall (2007), we calculate the total snow-albedo feedback (referred to hereafter as NET) from both the seasonal cycle and climate change according to equation (2) and its two components (SNC and TEM) from the seasonal cycle only according to equations (3) and (4). The partition of NET into SNC and TEM has a theoretical basis—namely, that the total snow-albedo feedback is controlled by these two mechanisms: reduction in surface albedo due to a loss of snow cover and that due to temperature increase. More specifically, SNC denotes snow cover feedback—that is to say that an increase in air temperature results in a reduction in snow cover, which, in turn, leads to a decrease in surface albedo. TEM refers to the snowpack metamorphosis feedback—that an increase in air temperature results in a decrease in snow-covered albedo that occurs with constant snow cover (Fletcher et al., 2015; Qu & Hall, 2007). The reduction in surface albedo because of both feedbacks can result in a further increase in air temperature. The feedback of snow on climate through SNC can be mostly seen in prior studies linking observed snow cover evolution with global warming (Déry & Brown, 2007; Groisman et al., 1994). For example, Groisman et al. (1994) demonstrated that the retreat of snow cover extent in the extratropical land region from 1972 to 1992 had significant impacts on the radiative balance and led to an enhanced spring warming. TEM is also an important mechanism, which provides a positive feedback to temperature through a decrease in surface albedo (a warming-induced increase in meltwater and snow grain size) without changing snow cover. The magnitude of this effect on surface climate depends on the rate of snow metamorphosis with temperature, which varies with many factors including vegetation type, snow thickness, and snow impurities such as black carbon (Flanner et al., 2007; Aoki et al., 2011).

$$\mathrm{NET} = \Delta\alpha s \ /\Delta T2\mathrm{m} \quad (2)$$

$$\mathrm{SNC} = (\alpha_{\mathrm{snow}} - \alpha_{\mathrm{land}})\ \Delta\mathrm{SCF}/\Delta T2\mathrm{m} \quad (3)$$

$$\mathrm{TEM} = \overline{\mathrm{SCF}}\ \ \Delta\alpha_{\mathrm{snow}}/\Delta T2\mathrm{m} \quad (4)$$

$$\alpha\mathrm{snow} = [\alpha s - \alpha\mathrm{land}\ (1 - \mathrm{SCF})]\ \ /\mathrm{SCF} \quad (5)$$

where Δ is the month to month change (from March to April, from April to May, and from May to June) in case of the seasonal cycle, or the difference in climatological mean March–May values between the current (1982–2005) and the future RCP 8.5 scenario (2070–2095) in case of climate change. The *overbar* denotes

the time averaged for spring months. SCF is the snow cover fraction, and T_{2m} is the 2 m temperature; α_{snow}, α_{land}, and α_s represent snow-covered, snow-free, and surface albedo, respectively. Here we use 10% as a threshold value of SCF (Fletcher et al., 2012) to calculate α_{snow} from α_{land} and α_s (equation (5)) since the choice of the relatively high values such as 25% adopted in Fletcher et al. (2015) would lead to a significant loss of pixels. α_{land} is computed by averaging surface albedo from July and August. All albedo values are weighted by incoming solar insolation, with insolation coming from each CMIP5 model for the modeled albedo, and ERA-I insolation for both satellite observations and ERA-I albedo.

2.4. Emergent Constraint on Future Modeled Snow-Albedo Feedback

We apply the similar constraint method with Cox et al. (2013) to first build the relationship between NET from the seasonal cycle and that from climate change under the unmitigated climate change scenario (RCP8.5) across CMIP5 models, and then use the satellite-derived NET from the seasonal cycle to produce a maximum-likelihood NET from climate change. Here probability density functions (PDFs) of climate change NET are calculated for the unconstrained CMIP5 models (prior PDF) and observationally constrained CMIP5 models (posterior PDF). The prior PDF is calculated by assuming that all CMIP5 models are equal and come from a Gaussian distribution. We follow the two steps in obtaining the posterior PDF. In the first step, we calculate the PDF of the observed seasonal cycle NET according to

$$P(x) = \frac{1}{\sqrt{2\pi\sigma_x^2}} \exp\left\{-\frac{(x-\overline{x})}{2\sigma_x}\right\} \tag{6}$$

where $\overline{x}$ is the mean seasonal cycle NET constructed through randomly selecting 18 years during the period 1982–2005 and σ_x is the corresponding standard error. In the second step, we calculate the prediction error (σ_f) of the linear least squares regression between y (climate change NET) and x (seasonal cycle NET) across CMIP5 models, which defines contours of equal probability density around the best fit linear regression, that represents the probability density of y given x.

$$P(y \mid x) = \frac{1}{\sqrt{2\pi\sigma_f^2}} \exp\left\{-\frac{y-f(x)}{2\sigma_f}\right\} \tag{7}$$

Given the PDFs $P(x)$ and $P(y \mid x)$, the observationally constrained PDF for y is

$$P(y) = \int_{-\infty}^{\infty} P(y \mid x)P(x)dx \tag{8}$$

More detailed information concerned with the constraint approach can be referenced to Cox et al. (2013).

The constraint will be applied over the Third Pole and in particular the following two regions: (1) the Karakoram region including the Karakoram, most of Pamir mountains, part of Hindu Kush mountains, and northwestern Himalaya Tibet (32°–39°N, 71°–79°E) and (2) the Southeastern Himalaya Tibet (referred to hereafter as Southeastern Tibet) (28°–36°N, 93°–103°E) (Figure 1). These two regions, with different moisture sources, are particularly considered since the winter precipitation on the Karakoram is influenced by winter westerlies and the precipitation on the Southeastern Tibet is affected by the Indian and Southeast Asian monsoons (Kapnick et al., 2014).

3. Results and Discussion

3.1. Quantitative Assessments of Satellite-Derived Snow Products

To understand whether the CMSAF product is suitable for quantifying the snow-albedo feedback, we evaluate the CMSAF albedo using in situ albedo measurements at the three stations (NAMOR, QOMS, and SETS) over the Tibetan Plateau (Table S1). Our results show that the CMSAF albedo in general captures the 5 day climatology of in situ albedo from March to June (N = 24), with the root-mean-square errors (RMSEs) being 0.08, 0.11, and 0.09 at NAMOR, QOMS, and SETS, respectively (Figure S1 in the supporting information). But the CMSAF appears to well capture the 5 day climatology of in situ albedo during the spring season at NAMOR and SETS stations instead of QOMS station (Figure S1). We should be cautious on the interpretation of this validation result. On the one hand, there is a mismatch in the spatial scale of the point-like observation at the site and the coarse resolution satellite retrieval. The spatial representativeness of the measured albedo at these stations is around 1 km (Qin et al., 2011), which is much finer than that of CMSAF albedo (~25 km).

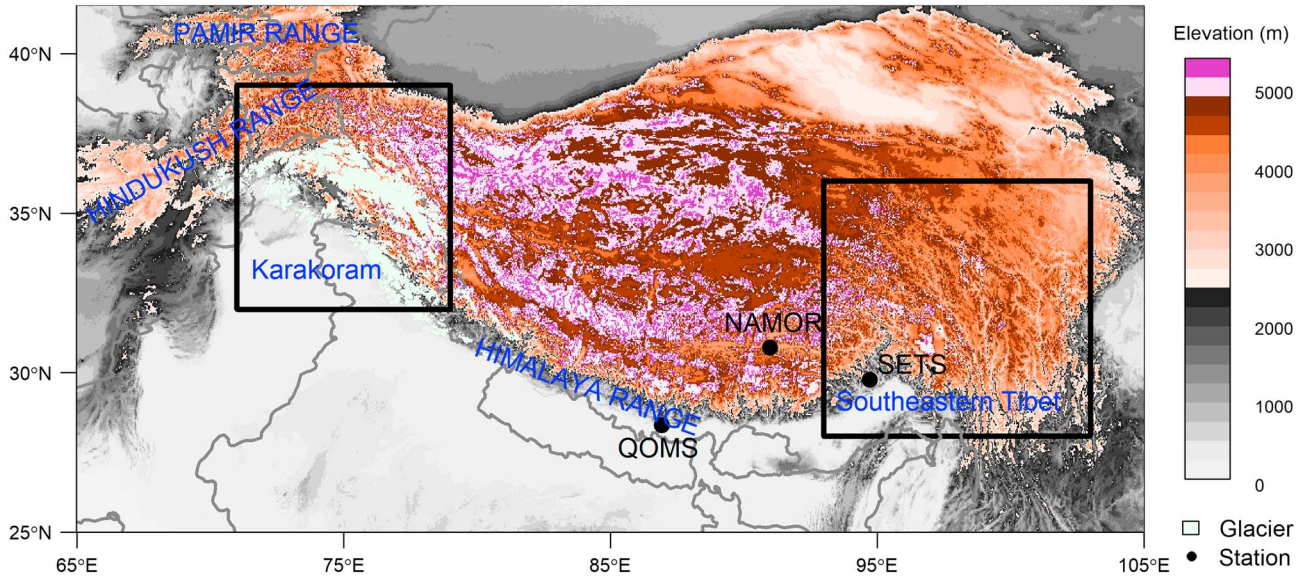

Figure 1. Orography of the Third Pole. The subregions including the Karakoram and Southeastern Tibet are outlined in black, and mountain glaciers are also shown.

According to vegetation map of the People's Republic of China (1:1000000) (Editorial Board of Vegetation Map of China, Chinese Academy of Sciences, 2007), the grid cell (~25 km) in which QOMS and SETS stations are located is not completely buried by snow, since 9.35% and 52.6% of the grid cell are covered by shrubs and forests (tall vegetation) at QOMS and SETS, respectively. By contrast, the main vegetation type at all of the three stations is reported to be the meadow type that can be completely buried by snow. The difference in land cover induced surface heterogeneity within the grid cell (~25 km) across stations could then partly account for the finding that NAMOR (low land cover heterogeneity) has a smaller RMSE than SETS and QOMS (high land cover heterogeneity) do. Another explanation is that the grid cells in which all stations are located are not fully covered by snow according to the MODIS SCF and NOAA-derived SCF data sets (Table S3). The snow cover fraction in the grid cell in which QOMS station is located is even below ~5%, which tentatively suggests that snow cover-induced surface heterogeneity would also be responsible for the high RMSE at the QOMS station. This conjecture is further supported by comparing CMSAF albedo with in situ albedo during the snow-free period. For example, the RMSE becomes smaller during July and August than that during the spring season, with its value being 0.06, 0.10, and 0.07 for NAMOR, QOMS, and SETS (N = 12), respectively. On the other hand, irradiation at validation sites contains atmospheric effects (such as aerosols and water vapor content) which could alter the spectral composition and albedo. But the CMSAF product provides a black-sky surface albedo without atmospheric effects. To achieve better comparability, in situ albedo should be corrected for atmospheric effects on irradiance, but the relevant information on aerosols and water vapor content of the atmosphere at these validation sites is not available.

Since the MODIS snow product is widely considered as a benchmark for other satellite-derived products (Dorothy & Riggs, 2007; Riggs & Hall, 2014), we thus adopt MODIS black-sky albedo and SCF to check the consistency between MODIS and CMSAF (and NOAA) over the Third Pole. Our analysis indicates that spatial patterns of multiyear (2000–2009) mean monthly albedo are broadly similar between CMSAF and MODIS from May to June (Figure S2). This result is similarly found between NOAA-derived SCF and MODIS SCF (Figure S3). In addition, both CMSAF and MODIS have high albedo values in the Karakoram and low ones in Southeastern Tibet. For example, the spatial mean albedo of CMSAF and MODIS is 0.41 ± 0.1 and 0.37 ± 0.08 in the Karakoram, and 0.28 ± 0.04 and 0.18 ± 0.05 in Southeastern Tibet. The observed larger CMSAF albedo than MODIS albedo in these two regions is in accord with the previous finding that the CMSAF albedo is typically 10–20% higher than the MODIS albedo (MCD43C3 product), because of the systematic retrieval uncertainty and the difference in aerosols and anisotropy correction (Riihelä et al., 2013). Moreover, the albedo difference between these two products is larger in Southeastern Tibet (~0.1) than that in Karakoram region (~0.04), which is partly related to the fact that Southeastern Tibet has a larger forest area (~20.2%) than the Karakoram region (~10.7%) does. This speculation is stimulated from the fact that the land

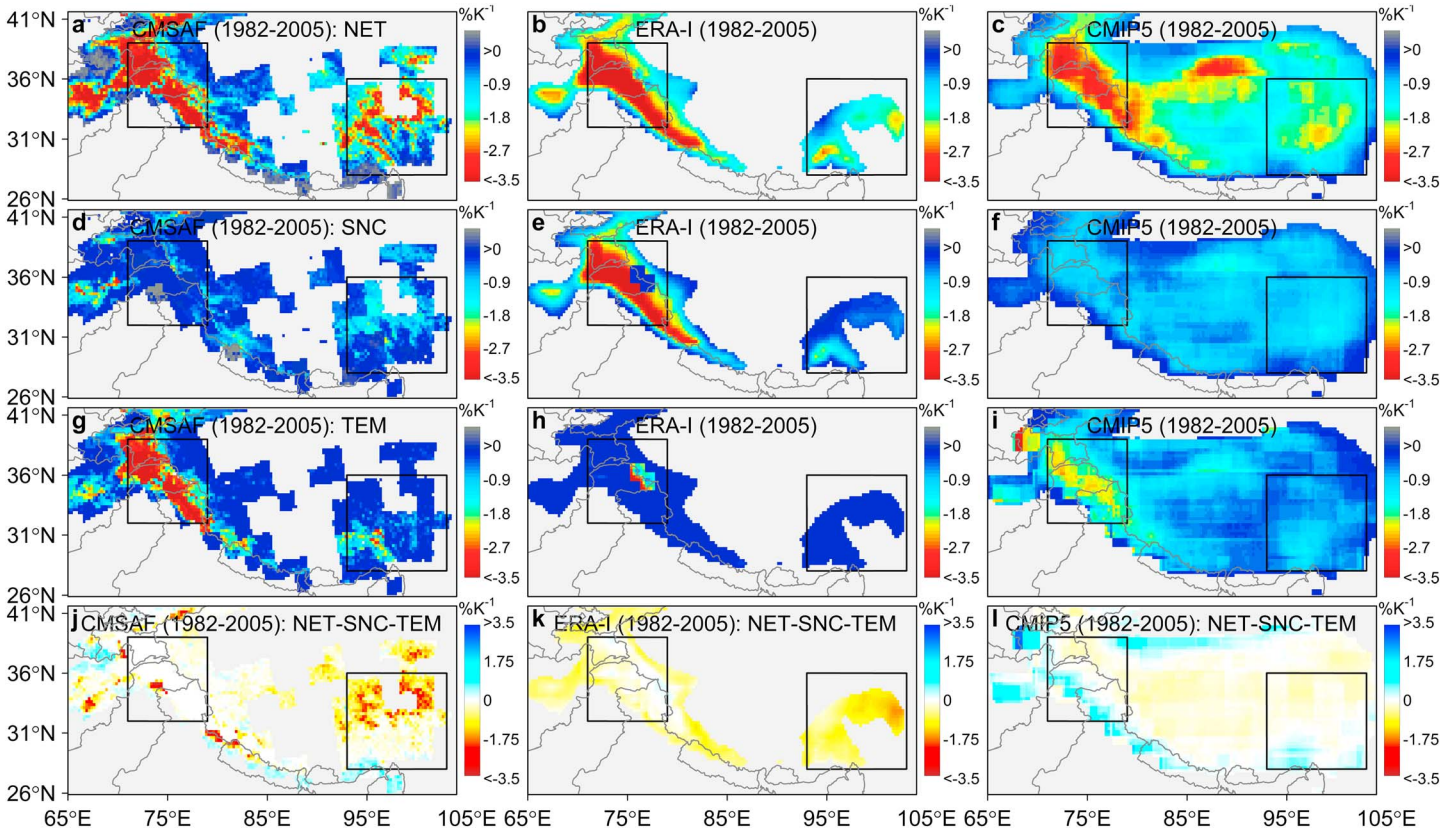

Figure 2. Spatial pattern of spring (March-April-May) climatological snow-albedo feedback (NET) and its two components (TEM and SNC) during the period 1982–2005 from (a, d, and g) CMSAF, (b, e, and h) ERA-I, and (c, f, and i) CMIP5 multimodel mean, respectively. (j–l) Difference between NET and the sum of SNC and TEM for CMSAF, ERA-I, and CMIP5 multimodel mean, respectively. NET, SNC, and TEM represent total snow-albedo feedback, snow cover feedback, and snowpack metamorphosis feedback.

cover data set used in the two albedo products is not the same, and they generally exhibit the high disagreement in the forests (Riihelä et al., 2013). The spatial mean SCF from NOAA and MODIS is 81% ± 5% and 77% ± 6% in the Karakoram and 49% ± 7% and 47% ± 3.2% in Southeastern Tibet. Moreover, there is a significant interannual correlation between CMSAF (NOAA-derived SCF) and MODIS, with the correlation coefficient being 0.72 (0.79) and 0.55 (0.54) in the Karakoram and Southeastern Tibet, respectively. Our quantitative assessment of CMSAF albedo and NOAA-derived SCF therefore adds confidence in the following snow-albedo feedback analysis.

3.2. Climatological Snow-Albedo Feedback and Its Two Components

Satellite-derived spring NET climatology, which is calculated based on CMSAF albedo and CRU temperature during the period 1982–2005, has a geographically nonuniform distribution, with large negative values mainly found in the Hindu Kush and Pamir mountains, in the region northwest of the Karakoram, in the western Himalayas, and in Southeastern Tibet (Figure 2a). For example, over the Karakoram, Southeastern Tibet, and the Third Pole, the spatial medians (25% and 75%) of NET (% K^{-1}) from CMSAF albedo are −2.7 (−3.75 and −1.03), −1.06 (−1.70 and −0.44), and −1.10 (−2.07 and −0.49), respectively. The spatial distribution of spring NET is roughly consistent with that of spring SCF and albedo (Figure S4), which is in accord with the previous finding that the effective snow albedo (defined as the albedo of 100% snow-covered surfaces that can be inferred from SCF and surface albedo according to equation (5)) determines the magnitude of NET (Qu & Hall, 2007). Consistently with the CMSAF (Figure 2a), large negative values of NET are similarly found in the Karakoram for both ERA-I (Figure 2b) and the multimodel ensemble mean (Figure 2c). Moreover, in terms of regional mean, the multimodel ensemble has a larger NET magnitude than CMSAF-derived value over Southeastern Tibet and the Third Pole but not over the Karakoram, and ERA-I shows a similar NET with the observation in the Karakoram but not over Southeastern Tibet and the Third Pole (Figure 3).

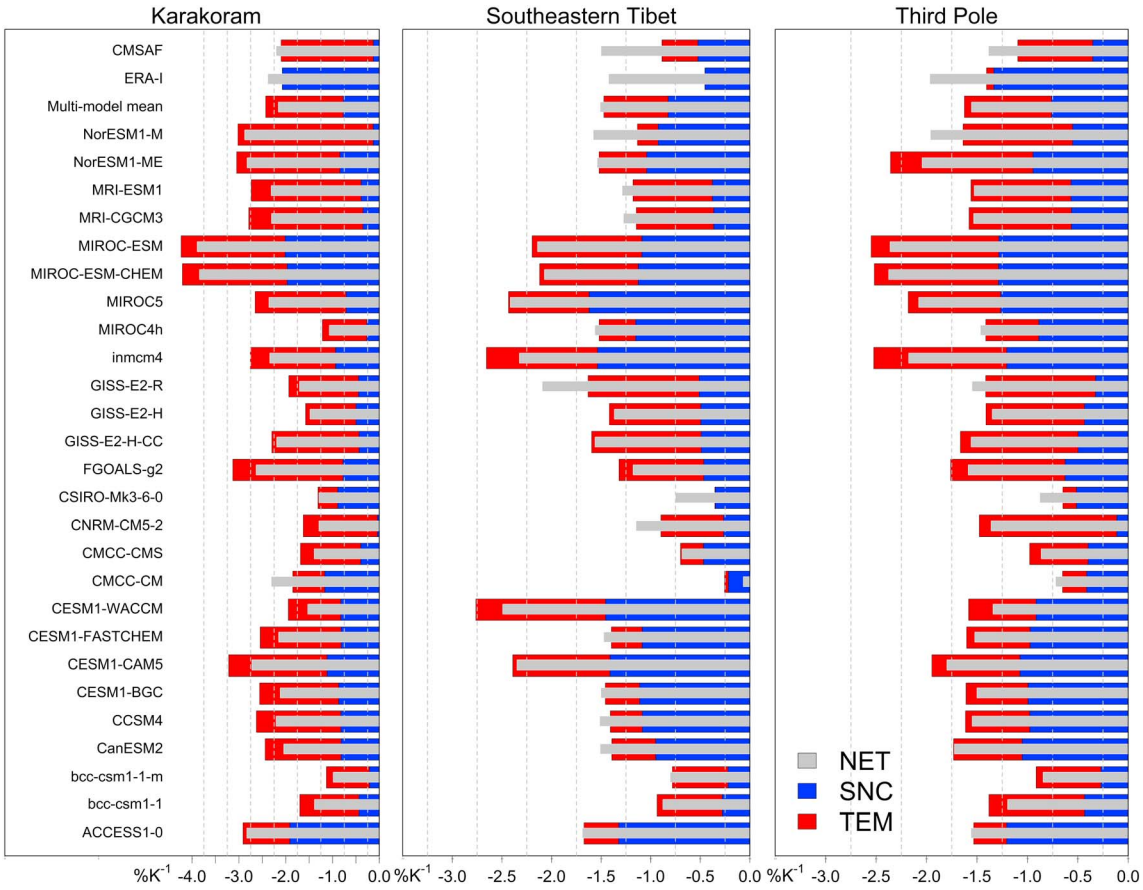

Figure 3. Comparison of spring (March-April-May) climatological snow-albedo feedback (NET) and its two components (SNC and TEM) during the period 1982–2005 between CMSAF, ERA-I, and CMIP5 over the Karakoram, Southeastern Tibet, and the Third Pole, respectively.

In addition, there is a large model spread in NET, with the largest value being approximately 4 times as large as the smallest (Figure 3). It is essential to mention that we do not calculate NET in pixels with SCF lower than 10%, but the NET from CMIP5 models still has that value over the whole Third Pole, since CMIP5 models generally have an unrealistically high spring SCF (Figure S4). The spatial decomposition of NET into SNC and TEM shows that NET is mainly driven by TEM in the Karakoram and by SNC in Southeastern Tibet, according to CMSAF albedo data (Figures 2d and 2g). Since the month-to-month SCF change (i.e., from March to April) is an important determinant of SNC according to equation (3), the SCF change based on NOAA in the Karakoram is not as dramatic as Southeastern Tibet (Figure S3). For example, based on NOAA, the SCF change from March to June is 12.4% in the Karakoram, which is lower than that (19%) in Southeastern Tibet. In addition, the albedo contrast also constitutes a factor in determining the magnitude of SNC. Compared to Southeastern Tibet, the Karakoram has a relatively high glaciated area (6.2% based upon the Randolph glacier inventory; Arendt et al., 2012), which could result in the low albedo contrast (then SNCs are of minor importance). In contrary to observations, SNC ($-2.07\%\ K^{-1}$) instead of TEM ($-0.002\%\ K^{-1}$) is found to predominate over NET ($-2.38\%\ K^{-1}$) from ERA-I data over the Karakoram (Figure 3). This pattern, which contrasts directly satellite-based analysis, can be explained by the fact that the month-to-month change in SCF is significantly more underestimated in ERA-I than is the case in NOAA-derived SCF over the Karakoram (Figure S3). For example, in the Karakoram, the SCF change from March to June is 54% in ERA-I, which is much higher than that (12.4%) in NOAA-derived SCF. But contributions from SNC and TEM terms to NET vary among CMIP5 models. For example, in the Karakoram region, of all 26 models, 3 have NET that is dominantly contributed by SNC, 20 have NET that is dominantly contributed by TEM, and 3 have NET nearly equally contributed by SNC and TEM (Figure 3).

It is important to note that the additivity of SNC and TEM equaling to NET indicates that the two components (i.e., snow albedo reduction due to snow metamorphosis and a loss of snow cover) would fully capture the physical processes controlling the total snow albedo feedback (Thackeray & Fletcher, 2016). This additivity is, however, not always satisfied at the pixel scale (Figures 2j–2l) or at the regional level (Figure 3). The lack of additivity is mainly found in Southeastern Tibet (Figure 2j). For example, in terms of regional mean, the NET in southeastern Tibet is approximately $-1.5\%\ K^{-1}$, with a contribution of $-0.52\%\ K^{-1}$ from SNC and $-0.36\%\ K^{-1}$ from TEM. In contrast, the additivity is well satisfied in the Karakoram as a whole, with NET, SNC, and TEM being $-2.1\%\ K^{-1}$, $-0.13\%\ K^{-1}$, and -2.0% K^{-1}, respectively. This nonadditivity is also found in prior studies (Fletcher et al., 2012; Fletcher et al., 2015). For example, Fletcher et al. (2015) showed that the additivity was satisfied at the hemispheric scale but not at the subhemispheric or latitudinal scales, using observational products. However, the exact reasons for this nonadditivity are still not clear. Thackeray and Fletcher (2016) speculated that this nonadditivity could be tied to the inaccuracies with satellite-derived SCF, since the calculation of SNC using equation (3) is sensitive to biases in the satellite-based SCF product. This speculation appears not to fully explain our results since the additivity is also not satisfied in southeastern Tibet using simulation results from CMIP5 models that can be assumed as physically consistent surrogates of the reality. Here another alternative explanation would be that the derivation of SNC is subject to the large uncertainty when SCF is relatively low, since estimation of the snow-covered albedo (surface albedo of 100% snow-covered surfaces) necessary for calculating SNC could become unstable in the relatively low SCF, particularly in southeastern Tibet (37 ± 20%) (Fletcher et al., 2015).

Finally, we also analyze changes in climatological NET from CMSAF along the altitudinal gradient by dividing the Third Pole into 10 elevation ranges with a 500 m interval and find that the strength of snow-albedo feedback increases rapidly (i.e., NET becomes more negative) for elevations less than 4,000 m and then increases slightly above 4,000 m (Figure 4a). This altitudinal pattern of snow-albedo feedback strength is generally consistent with that of observed warming rates over the last 30 years (Figure 4a). The warming can be ubiquitously observed across all elevation intervals, and the warming rate is found to be significantly ($P < 0.05$) correlated with climatological NET across pixels within each elevation interval ($R = -0.47 \pm -0.1$) as well as across all of the data ($R = -0.27$, $P < 0.05$) (Table S4). We thus tentatively suggest that snow-albedo feedback is a possible forcing for elevation-dependent warming during recent decades over the Third Pole. However, it should be noted that mere good correlations cannot be used to assign cause and effect. In addition, our results should not be overinterpreted particularly for high elevation areas (i.e., greater than 4,000 m), since in those regions, in situ stations are heavily undersampled in the generation of temperature data such as CRU.

Based on the same elevation data (the Shuttle Radar Topography Mission digital elevation data at a spatial resolution of 90 m) with the satellite-based analysis, the observed elevation-dependent pattern in snow-albedo feedback strength and warming rate (Figure 4a) is not similarly found in both ERA-I (Figure 4b) and CMIP5 model ensemble mean (Figure 4c). Note that this result is also found if the model-dependent elevation data were used (Figure S5). This mismatch might be possibly related to the use of a low-resolution model that has a relatively poor depiction of complex topography over the Third Pole. For example, Yan et al. (2016) ran the Community Climate System Model in experimental configurations with different model resolutions (T85: approximately 1.4° resolution and 256 × 128 regular longitude/latitude; T31: approximately 3.75° resolution and 96 × 48 regular longitude/latitude) and found that the elevation-dependent warming was only captured in the T85 resolution run. The model-data mismatch in elevation-dependent pattern cannot be solely explained by the adoption of the experimental configuration with a coarse spatial resolution, since some CMIP5 models (Table S2) and ERA-I have comparable, or even finer, spatial resolution than does the T85 resolution. We further show that the altitudinal distributions of surface albedo and snow cover fraction are not always consistent between ERA-I, the CMIP5 model ensemble, and the satellite-based products (Figure S6). This suggests that part of the model-data mismatch might be due to inaccuracies of snow simulations arising from model deficiencies in albedo and SCF parameterizations (Li et al., 2016; Qu & Hall, 2014; Wang et al., 2016). Moreover, elevation-dependent warming is a combination of various mechanisms including not only snow-albedo feedback but also cloud cover, water vapor, and aerosols (Pepin et al., 2015), and simulation accuracies in these processes might also play a certain role.

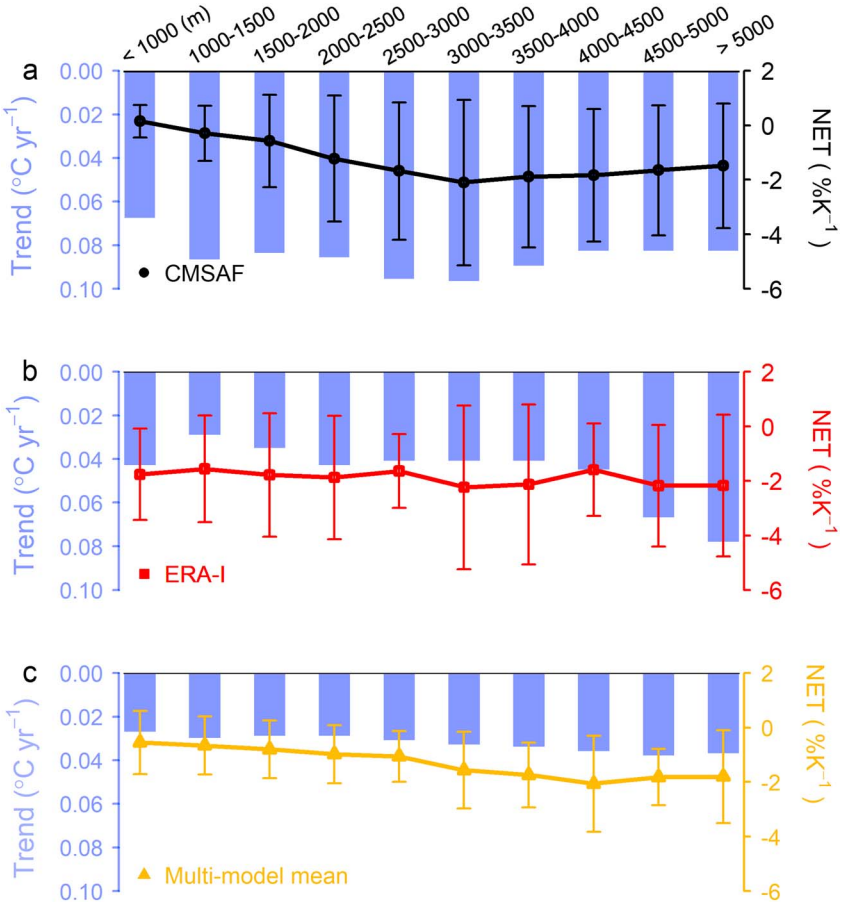

Figure 4. Elevational distribution of climatological snow-albedo feedback (NET) and the temperature trend during the period 1982–2005. (a) NET calculated from CMSAF albedo and CRU temperature. (b) NET calculated from ERA-I albedo and corresponding temperature. (c) NET calculated from CMIP5 multimodel mean albedo and corresponding temperature. The altitudinal gradient is constructed by dividing the Third Pole into 10 elevation ranges with a 500 m interval. The error bars represent interpixel standard deviation around the mean within each elevation range.

3.3. Using Satellite Earth Observations to Constrain Future Snow-Albedo Feedback

There is a large model spread in projected snow-albedo feedback in CMIP5 models, with the magnitude of NET (% K^{-1}) ranging from −1.57 to −4.06, from −0.08 to −2.55, and from −0.96 to −2.44 over the Karakoram, Southeastern Tibet, and the whole Third Pole under the unmitigated RCP8.5 scenario, respectively. The use of the multimodel ensemble mean is likely to provide a more robust estimate of NET under future climate change than any single model, but CMIP5 models have a systematic bias such as unrealistic high SCF and surface albedo during spring season over the Third Pole (Fletcher et al., 2015; Li et al., 2016). To have a robust estimate of future snow-albedo feedback, we thus adopt the emergent constraint method (Cox et al., 2013; Wenzel et al., 2016).

In consistency with previous studies (Hall & Qu, 2006), we also identify that NET calculated from the seasonal cycle is significantly correlated with that from climate change under the unmitigated scenario over the Karakoram (R^2 = 0.65, $P < 0.05$), Southeastern Tibet (R^2 = 0.65, $P < 0.05$), and the Third Pole (R^2 = 0.43, $P < 0.05$) across the entire ensemble of models (Figure 5). Then, using this model-based linear correlation, combined with satellite-based observations calculated from the seasonal cycle, we estimate a posterior probability density function (PDF) for future NET over different regions. Note that the prior PDF is calculated by assuming that CMIP5 models come from a Gaussian distribution (red line in Figure 5). The application of this emergent constraint moves the central estimate of future NET from −2.63 ± 0.76% K^{-1} to a less negative value (−2.42 ± 0.48% K^{-1}) over the Karakoram (Figures 5a and 5b). In contrast, the central estimate of future NET in Southeastern Tibet does not significantly change after the constraint, but with a reduced range of

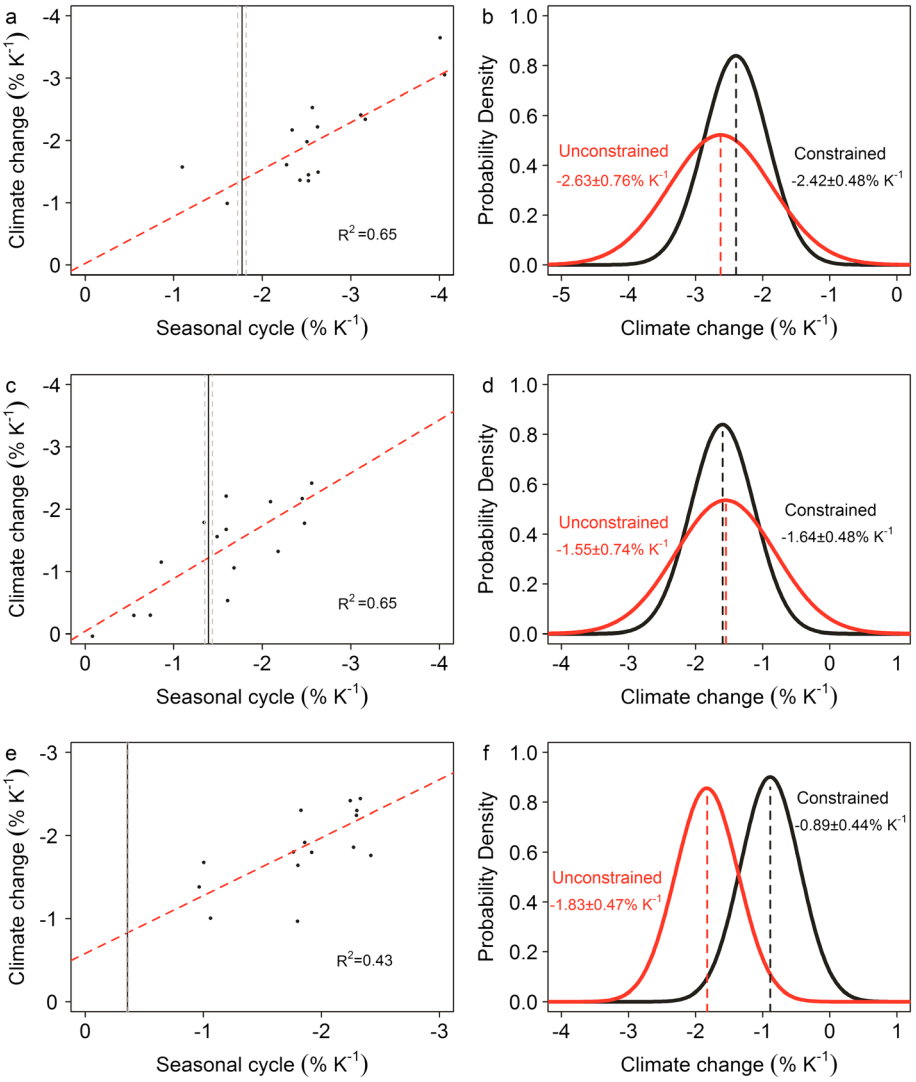

Figure 5. Observational constrained estimate of future snow-albedo feedback under unmitigated scenario. (a, c, and e) Relationship between NET calculated from seasonal cycle and that from future climate change across the ensemble of CMIP5 models over the Karakoram, Southeastern Tibet, and Third Pole, respectively. The black line indicates the NET calculated from the seasonal cycle based on CMSAF, and the gray dashed lines give the observational uncertainty that is constructed through randomly selecting 18 years during 1982–2005. (b, d, and f) Probability density function (PDF) of climate change NET under unmitigated scenario over the Karakoram, Southeastern Tibet, and Third Pole, respectively. The prior PDFs are derived by assuming all of the CMIP5 models are equally likely to be correct and that they come from a Gaussian distribution. The black line indicates the posterior PDF for climate change NET, which is derived by applying the observational constraint to the cross-model relationship shown in Figures 5a, 5c, and 5e.

uncertainty (unconstrained: $-1.55 \pm 0.74\%\ K^{-1}$; constrained: $-1.64 \pm 0.48\%\ K^{-1}$) (Figures 5c and 5d). Over the Third Pole, the emergent constraint also implies a reduced range of uncertainty for the future NET, with a central estimate of $-0.89 \pm 0.44\%\ K^{-1}$, that is also much lower than suggested by the unweighted CMIP5 models ($-1.83 \pm 0.47\%\ K^{-1}$) (Figures 5e and 5f). Our results indicate that future snow-albedo feedback strength over the Karakoram is nearly 1.5 and 3 times as strong as that over Southeastern Tibet and the Third Pole, respectively. Because of the strong spring snow-albedo feedback on temperature over the Karakoram, the present-day "Karakoram glacier anomaly" (the glaciers in the Karakoram mountains remained stable and even increased in recent decades) (Picard et al., 2012; Yao et al., 2012) might, in the future, switch to a "more normal" state (i.e., glacier melting due to temperature increases exceeds glacier accumulation due to snowfall increases). We should keep in mind that our observational-constrained estimate of future NET is still subject to uncertainties, since current CMIP5 models in general fail to

account for some processes such as the effect of snow impurities on albedo, physically based snow grain metamorphism.

4. Conclusions and Perspectives

This is the first study to utilize the long-term albedo data to systematically quantify the strength of snow-albedo feedback over the Third Pole, where rapid changes in the cryosphere were still under way. There is a large spatial heterogeneity in the total snow-albedo feedback over the Third Pole, with the largest feedback strength observed over most parts of the Karakoram. This strong feedback strength is primarily determined by the snowpack metamorphosis feedback (a warming-induced decrease in snow-covered albedo that occurs with constant snow cover) instead of snow cover feedback (a warming-induced decrease in snow cover and then surface albedo). We also demonstrate emergent constraints on snow-albedo feedback in the future climate change, using satellite-observed snow-albedo feedback strength calculated based on the seasonal cycle. The constrained future feedback strength is significantly different from the unconstrained model estimate particularly over the Karakoram and the Third Pole, indicating that the current climate models mostly bias the feedback of spring snow change to temperature change based on the future unmitigated scenario. It therefore cautions the direct use of spring temperature projections from CMIP5 model ensemble in quantifying climate change impacts on hydrological and ecological processes over the Third Pole. But our results could still suffer from certain uncertainties. For example, the quantification of snow-albedo feedback strength necessiates a robust gridded climate data, which is, however, difficult to reliably obtain over the Third Pole, with its complex topography and limited access.

In addition to these factors, there are further issues that need to be examined in future studies. First, the exact role of snow-albedo feedback in recent temperature change over the Third Pole is not known. This issue will be explored in our future studies through assimilating satellite observations in a coupled atmosphere-land variable-resolution global model (Wang et al., 2015). Second, although the altitudinal distribution of climatological snow-albedo feedback is consistent with that of warming rate for the last 30 years, this association does not imply causation and quantifying the accurate role of snow-albedo feedback mechanism in elevation-dependent warming necessiates the deployment of meteorological stations along an altitudinal gradient over the Third Pole (Pepin et al., 2015). This will be fairly resolved in future studies, since our Tibetan Plateau institute is now promoting the establishment of automatic climatic stations. Third, the Third Pole is experiencing increasing air pollution such as black carbon aerosols from the surrounding regions (Li et al., 2016), but the exact role of this pollution in changing snow-albedo feedback strength is still poorly known. Fourthly, although the emergent constraint method is adopted to estimate the future snow-albedo feedback from current state-of-the-art models, these models are still too coarse in accurately representing the role of topography and lacking in parameterizing critical snow physical processes.

Acknowledgments
This study was supported by National Natural Science Foundation of China (grants 41530528 and 41661144043), Key Research and Development Programs for Global Change and Adaptation (grant 2017YFA0603604), Key Research Program of Frontier Sciences of Chinese Academy of Sciences (grant QYZDJ-SSW-DQC019), International Partnership Program of Chinese Academy of Sciences (grant 131C11KYSB20160061), and the Thousand Youth Talents Plan project in China. The long-term albedo data from CLARA-A1-SAL, weekly NOAA/NCDC snow cover fraction, and MOD10CM (version 6) snow cover data can be downloaded from http://www.cmsaf.eu, https://data.nodc.noaa.gov/cgi-bin/iso?id=gov.noaa.ncdc:C00756, and https://nsidc.org/data/mod10cm, respectively. Temperature at 2 m from CRU TS3.2 can be obtained from https://crudata.uea.ac.uk/cru/data/hrg/. The elevation data set SRTM 90 m is freely available from http://srtm.csi.cgiar.org/SELECTION/inputCoord.asp. All variables from ERA-Interim data set can be downloaded from http://ecmwf.int/en/research/climate-reanalysis/erainterim. Earth system model (ESM) outputs to support this article are freely available from the CMIP5 repository (http://browse.ceda.ac.uk/browse/badc/cmip5/).

References

Aoki, T., Kuchiki, K., Niwano, K. M., Kodama, Y. J., & Hosaka, M. (2011). Physically based snow albedo model for calculating broadband albedos and the solar heating profile in snowpack for general circulation models. *Journal of Geophysical Research*, *116*, D11114. https://doi.org/10.1029/2010JD015507

Arendt, A., Bliss, A., Bolch, T., Cogley, J. G., Gardner, A. S., … Zheltyhina, N. (2012). *Randolph Glacier Inventory [v2.0]: A Dataset of Global Glacier Outlines*. Boulder Colorado, USA, Digital Media: Global land ice measurements from space.

Blanford, H. F. (1884). On the connection of the Himalaya snowfall with dry winds and seasons of drought in India. *Proceedings. Royal Society of London*, *37*(232-234), 3–22. https://doi.org/10.1098/rspl.1884.0003

Brown, R. D., & Robinson, D. A. (2011). Northern Hemisphere spring snow cover variability and change over 1922–2010 including an assessment of uncertainty. *The Cryosphere*, *5*, 219–229. https://doi.org/10.5194/tc-5-219-2011

Cox, P. M., Pearson, D., Booth, B. B., Friedlingstein, P., Huntingford, C., Jones, C. D., & Luke, C. M. (2013). Sensitivity of tropical carbon to climate change constrained by carbon dioxide variability. *Nature*, *494*(7437), 341–344. https://doi.org/10.1038/nature11882

Dee, D. P., Uppala, S. M., Simmons, A. J., Berrisford, P., Poli, P., Kobayashi, S., … Vitart, F. (2011). The ERA-Interim reanalysis: Configuration and performance of the data assimilation system. *Quarterly Journal of the Royal Meteorological Society*, *137*, 553–597. https://doi.org/10.1002/qj.828

Déry, S. J., & Brown, R. D. (2007). Recent Northern Hemisphere snow cover extent implications for the snow-albedo feedback. *Geophysical Research Letters*, *34*, L22504. https://doi.org/10.1029/2007GL031474

Dorothy, K. H., & Riggs, A. (2007). Accuracy assessment of the MODIS snow products. *Hydrological Processes*, *21*, 1534–1547. https://doi.org/10.1002/hyp.6715

Drusch, M., Vasiljevic, D., & Viterbo, P. (2004). ECMWF's global snow analysis: Assessment and revision based on satellite observations. *Journal of Applied Meteorology*, *43*, 1282–1294. https://doi.org/10.1175/1520-0450(2004)043%3C1282:EGSAAA%3E2.0.CO;2

Editorial Board of Vegetation Map of China, Chinese Academy of Sciences (2007). *Vegetation Map of the People's Republic of China (1:1000000) (Digital Version)*. Beijing, China: Geology Press.

Fasullo, J. (2004). A stratified diagnosis of the Indian monsoon-Eurasian snow cover relationship. *Journal of Climate*, *17*, 1110–1122. https://doi.org/10.1175/15200442(2004)017%3C1110:ASDOTI%3E2.0.CO;2

Flanner, M. G., Zender, C. S., Randerson, J. T., & Rasch, P. J. (2007). Present-day climate forcing and response from black carbon in snow. *Journal of Geophysical Research*, *112*, D11202. https://doi.org/10.1029/2006JD008003

Fletcher, C. G., Zhao, H. X., Kushner, P. J., & Fernandes, R. (2012). Using models and satellite observations to evaluate the strength of snow albedo feedback. *Journal of Geophysical Research*, *117*, D11117. https://doi.org/10.1029/2012JD177724

Fletcher, C. G., Thackeray, C. W., & Burgers, T. M. (2015). Evaluating biases in simulated snow albedo feedback in two generations of climate models. *Journal of Geophysical Research: Atmospheres*, *120*, 12–26. https://doi.org/10.1002/2014JD022546

Groisman, P. Y., Karl, T. R., Knight, R. W., & Stenchikov, G. L. (1994). Changes of snow cover, temperature, and radiative heat-balance over the Northern Hemisphere. *Journal of Climate*, *7*(11), 1633–1656. https://doi.org/10.1175/1520-0442(1994)007%3C1633:COSCTA%3E2.0.CO;2

Hall, A., & Qu, X. (2006). Using the current seasonal cycle to constrain snow albedo feedback in future climate change. *Geophysical Research Letters*, *33*, L03502. https://doi.org/10.1029/2005GL025127

He, T., Liang, S. l., & Song, D. X. (2014). Analysis of global land surface albedo climatology and spatial-temporal variation during 1981–2010 from multiple satellite products. *Journal of Geophysical Research: Atmospheres*, *119*, 10,281–10,298. https://doi.org/10.1002/2014JD021667

Helfrich, S. R., McNamara, D., Ramsay, B. H., Baldwin, T., & Kasheta, T. (2007). Enhancements to, and forthcoming developments in the interactive multisensor snow and ice mapping system (IMS). *Hydrological Processes*, *21*, 1576–1586. https://doi.org/10.1002/hyp.6720

Kang, S. C., Xu, Y. W., You, Q. L., Flugel, W. A., Pepin, N., & Yao, T. D. (2010). Review of climate and cryospheric change in the Tibetan Plateau. *Environmental Research Letters*, *5*, 015101. https://doi.org/10.1088/1748-9326/5/1/015101

Kapnick, S. B., Delworth, T. L., Ashfaq, M., Malyshev, S., & Milly, P. C. (2014). Snowfall less sensitivity to warming in Karakoram than in Himalayas due to a unique seasonal cycle. *Nature Geoscience*, *7*(11), 834–840. https://doi.org/10.1038/ngeo2269

Karlsson, K. G., Riihelä, A., Müller, R., Meirink, J. F., Sedlar, M., Lockhoff, M., … Wolters, E. (2013). CLARA-A1: A cloud, albedo, and radiation dataset from 28 yr of global AVHRR data. *Atmospheric Chemistry and Physics*, *13*(1), 935–982. https://doi.org/10.5194/acpd-13-935-2013

Kumar, P., Kotlarski, S., Moseley, C., Sieck, K., Frey, H., Stoffel, M., & Jacob, D. (2015). Response of Karakoram-Himalayan glaciers to climate variability and climatic change: A regional climate model assessment. *Geophysical Research Letters*, *42*, 1818–1825. https://doi.org/10.1002/2015GL063392

Kwiatkowski, L., Bopp, L., Aumont, O., Philippe, C., Cox, P. M., Laufkötter, C., … Séférian, R. (2017). Emergent constrains on projections of declining primary production in the tropical oceans. *Nature Climate Change*, *7*(5), 355–358. https://doi.org/10.1038/nclimate3265

Li, Y., Wang, T., Zeng, Z. Z., Peng, S. S., Lian, X., & Piao, S. L. (2016). Evaluating biases in simulated land surface albedo from CMIP5 global climate models. *Journal of Geophysical Research: Atmospheres*, *121*, 6178–6190. https://doi.org/10.1002/2016JD024774

Lin, H., & Wu, Z. W. (2012). Contribution of Tibetan Plateau snow cover to the extreme winter conditions of 2009/10. *Atmosphere-Ocean*, *50*, 86–94. https://doi.org/10.1080/07055900.2011.649036

Liu, J. C., Schaaf, C., Strahler, A., Jiao, Z. T., Shuai, Y. M., Zhang, Q. L., … Dutton, E. G. (2009). Validation of Moderate Resolution Imaging Spectroradiometer (MODIS) albedo retrieval algorithm: Dependence of albedo on solar zenith angle. *Journal of Geophysical Research*, *114*, D01106. https://doi.org/10.1029/2008JD009969

Liu, X. D., Cheng, Z. G., Yan, L. B., & Yin, Z. Y. (2009). Elevation dependency of recent and future minimum surface air temperature trends in the Tibetan Plateau and its surroundings. *Global and Planetary Change*, *68*, 164–174. https://doi.org/10.1016/j.gloplacha.2009.03.017

Ma, Y. M., Zhong, L., Wang, B., Ma, W., Chen, X., & Li, M. (2011). Determination of land surface heat fluxes over heterogeneous landscape of the Tibetan Plateau by using the MODIS and in situ data. *Atmospheric Chemistry and Physics*, *11*, 10,461–10,469. https://doi.org/10.5194/acp-11-10461-2011

Manninen, T., Riihelä, A., & de Leeuw, G. (2012). Atmospheric effect on the ground-based measurements of broadband surface albedo. *Atmospheric Measurement Techniques*, *5*, 2675–2688. https://doi.org/10.5194/amt-5-2675-2012

Ménégoz, X., Krinner, G., Balkanski, Y., Boucher, O., Cozic, A., Lim, S., … Jacobi, H. W. (2014). Snow cover sensitivity to black carbon deposition in the Himalayas: From atmospheric and ice core measurements to regional climate simulations. *Atmospheric Chemistry and Physics*, *14*(8), 4237–4249. https://doi.org/10.5194/acp-14-4237-2014

Mitchell, T. D., & Jones, P. D. (2005). An improved method of constructing a database of monthly climate observations and associated high-resolution grids. *International Journal of Climatology*, *25*(6), 693–712. https://doi.org/10.1002/joc.1881

New, M., Hulme, M., & Jones, P. (1999). Representing twentieth-century space-time climate variability. Part I: Development of a 1961–90 mean monthly terrestrial climatology. *Journal of Climate*, *12*(3), 829–856. https://doi.org/10.1175/1520-0442(1999)012%3C0829:RTCSTC%3E2.0.CO;2

Niu, G. Y., & Yang, Z. L. (2007). An observation-based formulation of snow cover fraction and its evaluation over large North American river basins. *Journal of Geophysical Research*, *112*, D21101. https://doi.org/10.1029/2007JD008674

Pepin, N., Bradley, R. S., Diaz, H. F., Baraer, M., Caceres, E. B., Forsythe, N., … Yang, D. Q. (2015). Elevation-dependent warming in mountain regions of the world. *Nature Climate Change*, *5*(5), 424–430.

Picard, G., Domine, F., Krinner, G., Arnaud, L., & Lefebvre, E. (2012). Inhibition of the positive snow-albedo feedback by precipitation in interior Antarctica. *Nature Climate Change*, *2*(11), 795–798. https://doi.org/10.1038/nclimate1590

Pithan, F., & Mauritsen, T. (2014). Arctic amplification dominated by temperature feedbacks in contemporary climate models. *Nature Geoscience*, *7*(3), 181–184. https://doi.org/10.1038/ngeo2071

Pu, Z., Xu, L., & Salomonson, V. V. (2007). MODIS/Terra observed seasonal variations of snow cover over the Tibetan Plateau. *Geophysical Research Letters*, *34*, L06706. https://doi.org/10.1029/2007GL029262

Qin, J., Yang, K., Liang, S. L., & Guo, X. F. (2009). The altitudinal dependence of recent rapid warming over the Tibetan Plateau. *Climatic Change*, *97*, 321–327. https://doi.org/10.1007/s10584-009-9733-9

Qin, J., Yang, K., Liang, S. L., Zhang, H., Ma, Y. M., Guo, X. F., & Chen, Z. Q. (2011). Evaluation of surface albedo from GEWEX-SRB and ISCCP-FD data against validated MODIS product over Tibetan Plateau. *Journal of Geophysical Research*, *116*, D24116. https://doi.org/10.1029/20011JD015823

Qiu, J. (2008). China: The Third Pole. *Nature*, *454*, 393–396. https://doi.org/10.1038/454393a

Qu, X., & Hall, A. (2007). What controls the strength of snow-albedo feedback? *Journal of Climate*, *20*, 3971–3981. https://doi.org/10.1175/JCLI4186.1

Qu, X., & Hall, A. (2014). On the persistent spread in snow-albedo feedback. *Climate Dynamics*, *42*(1-2), 69–81. https://doi.org/10.1007/s00382-013-1774-0

Rangwala, I., & Miller, J. R. (2012). Climate change in mountains: A review of elevation-dependent warming and its possible causes. *Climatic Change*, *114*, 527–547. https://doi.org/10.1007/s10584-012-0419-3

Riggs, G. A., & Hall, D. K. (2014). Tracking seasonal Appalachian snow cover with MODIS daily snow cover product. In *Proceedings of the 71st Annual Eastern Snow Conference* (pp. 121–129). 3–5 June 2014. BOONE, NC.

Riihelä, A., Manninen, T., Laine, V., Andersson, K., & Kaspar, F. (2013). CLARA-SAL: A global 28 yr time series of Earth's black-sky surface albedo. *Atmospheric Chemistry and Physics*, *13*(7), 3743–3762. https://doi.org/10.5194/acp-13-3743-2013

Robinson, D. A., Estilow, T. W., & NOAA CDR Program (2012). NOAA climate date record (CDR) of Northern Hemisphere (NH) snow cover extent (SCE), version 1. NOAA National Climatic Data Center. https://doi.org/10.7289/V5N0114G9

Seol, K. H., & Hong, S. Y. (2009). Relationship between the Tibetan snow in spring and the East Asian summer monsoon in 2003: A global and regional modeling study. *Journal of Climate*, *22*, 2095–2110. https://doi.org/10.1175/2008JCLI2496.1

Taylor, K. E., Stouffer, R. J., & Meehl, G. A. (2012). An overview of Cmip5 and the experiment design. *B. A. M. S.*, *93*(4), 485–498. https://doi.org/10.1175/BAMS-D-11-00094.1

Thackeray, C. W., & Fletcher, C. G. (2016). Snow albedo feedback: Current knowledge, importance, outstanding issues and future directions. *Progress in Physical Geography*, *40*(3), 392–408. https://doi.org/10.1177/0309133315620999

Wallace, J. M. (1992). Physics of climate—Peixoto, Jp, Oort, Ah. *Nature*, *360*(6401), 220–220. https://doi.org/10.1038/360220a0

Wang, T., Peng, S. S., Krinner, G., Ryder, J., Li, Y., Dantec-Nedelec, S., & Ottle, C. (2015). Impacts of satellite-based snow albedo assimilation on offline and coupled land surface model simulations. *PLoS One*, *10*(9), e0137275. https://doi.org/10.1371/journal.pone.0137275

Wang, L., Cole, J. N. S., Bartlett, P., Verseghy, D., Derksen, C., Brown, R., & Salzen von, K. (2016). Investigating the spread in surface albedo for snow-covered forests in CMIP5 models. *Journal of Geophysical Research: Atmospheres*, *121*, 1104–1119. https://doi.org/10.1002/2015JD023824

Wenzel, S., Cox, P. M., Eyring, V., & Friedlingstein, P. (2016). Projected land photosynthesis constrained by changes in the seasonal cycle of atmospheric CO_2. *Nature*, *538*(7626), 499–501. https://doi.org/10.1038/nature19772

Xu, B. Q., Cao, J. J., James, H., Yao, T. D., Daninel, R. J., Wang, N. L., … He, J. Q. (2009). Black soot and the survival of Tibetan glaciers. *Proceedings of the National Academy of Sciences of the United States of America*, *106*(52), 22,114–22,118. https://doi.org/10.1073/pnas.0910444106

Yan, L. B., Liu, Z. Y., Chen, G. S., Kutzbach, J. E., & Liu, X. D. (2016). Mechanisms of elevation-dependent warming over the Tibetan plateau in quadrupled CO_2 experiments. *Climatic Change*, *135*(3-4), 509–519. https://doi.org/10.1007/s10584-016-1599-z

Yang, W., Guo, X. F., Yao, T. D., Zhu, M. L., & Wang, Y. J. (2016). Recent accelerating mass loss of southeast Tibetan glaciers and the relationship with changes in macroscale atmospheric circulations. *Climate Dynamics*, *47*(3–4), 805–815. https://doi.org/10.1007/s00382-015-2872-y

Yao, T. D., Lonnie, T., Yang, W., Yu, W. S., Gao, Y., Guo, X. J., … Daniel, J. (2012). Different glacier status with atmospheric circulations in Tibetan Plateau and surroundings. *Nature Climate Change*, *2*, 663–667. https://doi.org/10.1038/nclimate1580

Zeng, Z. Z., Chen, A. P., Philippe, C., Li, Y., Laurent, Z. X., Vautard, R., … Piao, S. L. (2015). Regional air pollution brightening reverses the greenhouse gases induced warming-elevation relationship. *Geophysical Research Letters*, *42*, 4563–4572. https://doi.org/10.1002/2015GL064410

Zhao, C., Piao, S. L., Wang, X. H., Huang, Y., Philippe, C., Joshua, E., … Josep, P. (2017). Plausible rice yield losses under future climate warming. *Natural Plants*, *3*, 16202. https://doi.org/10.1038/nplants.2016.202

Zhong, L., Su, Z. B., Ma, Y. M., Salama, M. S., & Sobrino, J. A. (2011). Accelerated changes of environmental conditions on the Tibetan Plateau caused by climate change. *Journal of Climate*, *24*, 6540–6550. https://doi.org/10.1175/JCLI-D-10-05000.1